Int. J. Electrochem. Sci., 13 **(2018)** 4548 – 4560, doi: 10.20964/2018.05.08

International Journal of ELECTROCHEMICAL SCIENCE
www.electrochemsci.org

Photoelectrocatalytic Oxidation of Phenol on Silver Loaded TiO_2 Nanotube Array at High Oxygen Pressure under Luminescent Light Irradiation

Farid F. Orudzhev[1,*], *A.B. Isaev*[1,*], *N.S. Shabanov*[1, 2], *F.G. Gasanova*[1], *A.Kh. Idrisova*[1], *D.P. Babaeva*[1]

[1] Dagestan State University, Russian Federation, Makhachkala, M. Gadjieva str. 43 a, 367001.
[2] Analytical Center for Collective Use, Dagestan Scientific Center, Russian Academy of Sciences, Russian Federation, Makhachkala, M. Gadjieva str. 45, 367000,.
[*]E-mail: ff.orudzhev@dgu.ru; abdul-77@yandex.ru

Received: 8 January 2018 / *Accepted:* 22 February 2018 / *Published:* 10 April 2018

TiO_2 and Ag-TiO_2/Ti-nanotubes were synthesized by electrochemical anodization and UV-light illumination photoreduction methods respectively. Scanning electron microscopy, X-ray diffraction and UV–vis spectrometry were used to characterize the nanotubes. Compared with pure TiO_2, Ag loaded TiO_2 showed higher visible light absorption activity. The characterization results indicate that the surface of the TiO_2 nanotubes partially coated with Ag nanoparticles with an average size of about 50-80 nm. The behavior of phenol at the Ag-TiO_2/Ti nanotubes array photoanode was characterized by linear voltammetry. We have investigated the effect of oxygen pressure to photoelectrocatalytic oxidation of phenol on Ag loaded TiO_2 nanotubes under luminescent light irradiation. Results show that the initial rate of oxidation increases with increasing oxygen pressure. Raising the oxygen pressure in the system from 0.1 to 0.6 MPa caused the initial rate of the photoelectrocatalytic phenol oxidation to increase nearly 1.4 times.

Keywords: photoelectrocatalytic, oxygen, phenol, oxidation, Ag loaded TiO_2 nanotubes.

1. INTRODUCTION

Since the beginning of the 1990-s, the photoelectrocatalysis has attracted increasing attention as one of the most effective methods in the field of environmental protection for remediation of the environment-degrading organic pollutants [1–4]. TiO_2 has been widely used among the variety of semiconducting metal oxides as the photocatalyst. TiO_2 is the most useful photocatalyst due to its low cost, non-toxicity, large stability and high activity during the oxidation of organic compounds [5–9].

It is well known that nanoscale materials have the physical and chemical properties which vary in dependence on the size and geometry of nanomaterials and therefore nanotubes are of great interest. The application of nanostructured materials, such as nanotubes, in photocatalytic degradation of organic pollutants and the mechanisms which involve these processes, have also been discussed in the literature [10–15]. TiO_2 nanotubes have attracted a lot of attention due to their high surface area and extraordinary characteristics for application in photocatalysis, photoelectrolysis and photoelectrocatalysis [16,17].

However, the wide band-gap of anatase TiO_2 (3.2 eV) restricts its photocatalytic applications to the visible-light range [18]. The relatively high rate of electron-hole recombination often results in a low quantum yield and poor efficiency of photocatalytic reactions [19,20]. Most of the studies have been focused on the modification of TiO_2 nanotubes loaded by metal ions, especially transition metal ions, which makes possible for TiO_2 to absorb visible light by increasing the charge separation [21–25].

Silver is often used for TiO_2 modification to increase photocatalytic efficiency [26–31]. The silver nanoparticles, fixed on TiO_2 nanotubes, can act as electron traps and limit the recombination of electrons and holes. Silver has also other advantages including relatively low cost in comparison to other noble metals, bactericidal properties and high oxygen adsorption [25, 26]. Recently, some studies reported the Ag/TiO_2 composites on photocatalytic processes and demonstrated that it is more efficient in comparison to the pure TiO_2 [32]. The silver modification of highly oriented TiO_2 nanotube arrays and their application in photocatalysis and photoelectrocatalysis have also been studied [33–37].

This paper discusses the photoelectrocatalytic activity of silver modified TiO_2 nanotube array photoanode for oxidation of phenol. The influence of oxygen pressure on the efficiency of photoelectrocatalytic oxidation of phenol is investigated.

2. EXPERIMENTAL

TiO_2/Ti nanotube array electrode was prepared by a synthetic procedure which has been described by us in detail previously [38]. The Ag nanoparticles were deposited on the surface of TiO_2 nanotube array electrode by UV-light illumination photoreduction from an aqueous solution containing 5 mM $AgNO_3$. The TiO_2 nanotube array electrode kept into the $AgNO_3$ solution for 12 h in dark at vacuum. Then the TiO_2 nanotube array electrode was illuminated under a UV-lamp for 30 min to carry the photoreduction. Then the Ag-TiO_2/Ti nanotube array electrode was annealed in a muffle furnace at $500^{\circ}C$ for 1 h [34].

Characteristics of obtained nanotubes were performed using electron microscopy and X-ray analysis. X-ray diffraction (XRD) studies of synthesized catalysts were carried out at $25^{\circ}C$ using diffractometer Empyrean series 2 firms PANalytical with Cu Kα_1 radiation (k = 0.15406 nm). The operating voltage and current were 40 kV and 30 mA, respectively. The diffraction patterns were measured in the 2θ range of 5-90^0 with step size and the step time of 0.0260 and 197 s was used for data collection. Image of the surface of the synthesized sample was prepared using a scanning electron microscope LEO 1450 with analyzer ISYS and EDX system (Leica Micro-systems Wetzlar GmbH,

Germany). The absorption spectra in the UV and visible ranges were recorded on a UV 3600 Shimadzu (Japan) spectrophotometer.

The voltammetric experiments were performed in an autoclave-reactor using a three-electrode system with a platinum foil counter electrode (5), a saturated Ag/AgCl reference electrode (6) and a TiO_2 nanotube array work electrode (4) (Fig. 1). The prepared samples served as the working electrodes with a geometric area of 0,25 cm^2. The supply bias and work current were controlled using an IPC-pro MF potentiostat-galvanostat (Volta-Prom, Russia). The working electrode (4) was illuminated by the light from the luminescent lamp (10) through a quartz window (7) of one side of the cell. The quartz glass fixed with Teflon cover (3). For the supply of oxygen and measuring the pressure in the cell were respectively a valve (2) and a manometer (1). The autoclave is equipped with lead wires for current supply (9). The potential scanning rate was 100 mV/s. The voltammograms obtained and photoelectrocatalytic activity was studied in aqueous 0.1 M Na_2SO_4 electrolyte solution.

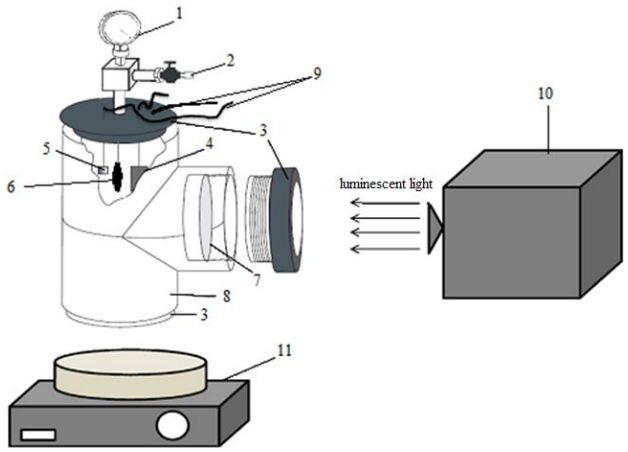

Figure 1. Schematic representation of the autoclave-electrolyser: 1 – manometer, 2 – gate, 3 – cover, 4 – TiO_2 nanotube work electrode, 5 – platinum foil counter electrode, 6 – reference electrode, 7 – quartz glass, 8 – Teflon body, 9 – lead wires, 10 – luminescent lamp, 11 – magnetic stirrer.

Photoelectrocatalytic activity of Ag-TiO_2/Ti nanotube array electrode was evaluated by degradation of phenol. Photoelectrocatalytic oxidation of phenol occurs at the expense of irradiation generated photocurrent without the supply bias to the cell [39]. The concentration of phenol in the solution was measured by the fluorimetric method in spectrofluorimeter Model “Fluorat 02 Panorama” (Russia).

3. RESULTS AND DISCUSSION

The SEM images and XRD patterns of Ag-TiO_2/Ti photoanode are shown in Fig. 2. From the SEM images (Fig. 2 (A)) the particle size of Ag deposited on TiO_2 nanotube varies from 50 to 80 nm. This could be due to agglomeration of some number of particles. The parameters of nanotubes of

titanium dioxide are not changed. However, it shows that their surface partially coated with nanoparticles. The amount of deposited silver was approximately 5%. The partial surface coating of Ag nanoparticles does not lead to any decrease in the absorption of light by the surface of the titanium dioxide. From the XRD patterns: the peak at $2\theta = 44.3^{o}$ and 64.21^{o} is characteristic to Ag metal, which confirms the deposition of Ag on the TiO_2 nanotube surface. The strongest peak in the Ag (111) plane is not observed, which perhaps could be masked by the Ti substrate peak $2\theta = 38.41^{o}$.

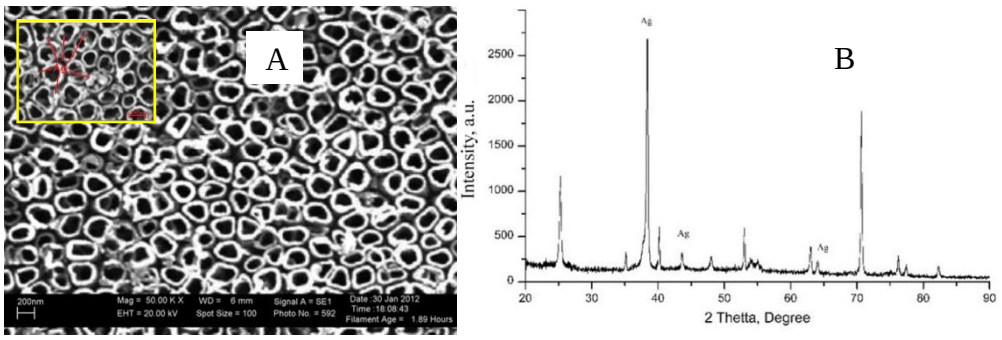

Figure 2. SEM image (A) and XRD pattern (B) for a sample of Ag-TiO_2/Ti nanotubes array photoanode.

Fig. 3 shows the UV-visible absorption spectra of pure TiO_2 nanotubes and Ag-TiO_2/Ti nanotubes array photoanode. Pure TiO_2 nanotubes photoanode shows absorption at UV region (100-200 *nm*). The Ag loaded TiO_2 nanotubes array photoanode showed the absorption corresponding to pure TiO_2 and also absorption between 320 and 450 nm. We estimated the band-gap energy of pure TiO_2 and Ag-TiO_2 nanotubes by the Kubelka–Munk relations (Fig. 3 (B). Band-gap energy of pure TiO_2 nanotubes was 3,2 *eV*. Ag loaded TiO_2 nanotubes showed a reduced band-gap of 2,1 *eV*.

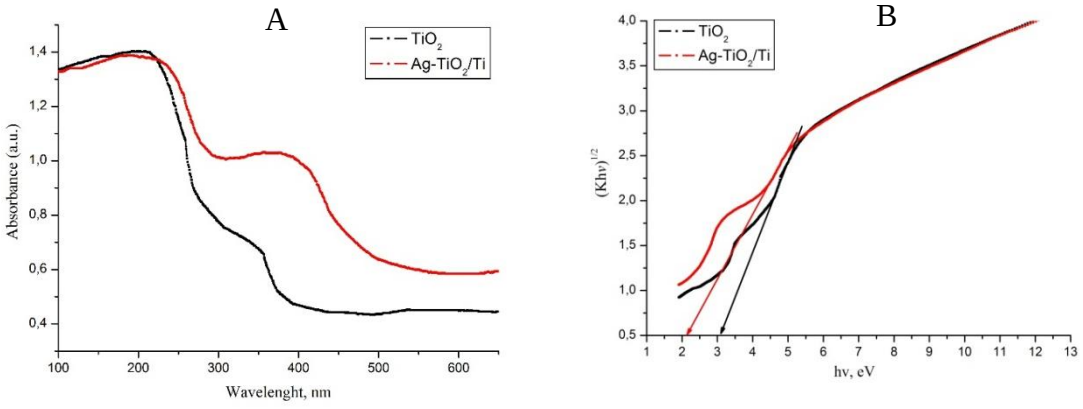

Figure 3. UV-visible absorption spectra of pure TiO_2 nanotubes and Ag-TiO_2/Ti nanotubes array photoanode (A) and its Kubelka-Munk plots (B).

The absorption edge at the wavelength of less than 320 nm can be attributed to self-absorption anatase bandgap. Spectra of modified samples show a slight shift of absorption to the large

wavelengths region. The similar effect for Pt, Pd, Ag and Au-Cu loaded TiO_2 samples was found in previous studies [18, 40–43]. The absorbance band in the visible range from 320 to 450 *nm* corresponded to the effect of plasmon resonance of silver nanoparticles [45]. With the aid of plasmon resonance effect, hot electrons were able to transfer from Ag nanocrystals into the conduction band of TiO_2 nanotubes [45, 46].

To evaluate the photoelectrocatalytic performance of Ag loaded TiO_2 nanotubes and separation of photoinduced charges when the fluorescent light irradiation the curves of the transient photocurrent was obtained. Chronoamperometric curves with the transient photocurrent are recorded in Fig. 4. As can be seen from the Fig. 4 the photocurrent under irradiation of fluorescent light for the Ag loaded TiO_2 photoanode drastically increases, due to the effect of plasmon resonance [46].

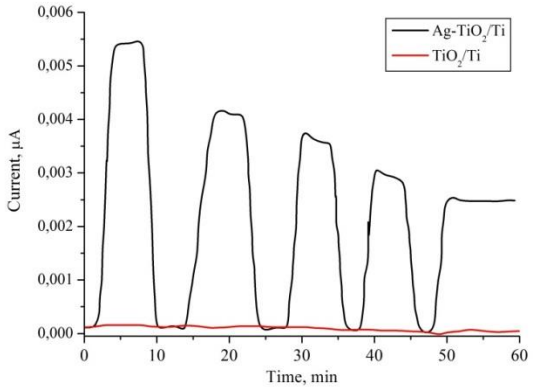

Figure 4. Photocurrent responses in the light on-off process under luminescent light irradiation.

The photogenerated electrons and holes on the surface of TiO_2 nanotubes react with H_2O and O_2 to form surface hydroxyl radical $HO^{\bullet}$ and $O_2^{\bullet-}$. The photogenerated electrons generate current in the external circuit in the photoelectrocatalytic process [48–51].

The photoelectrocatalytic process of Ag-TiO_2/Ti nanotubes anode can be described as follows [40]:

$$h^+ + HO^- \rightarrow HO^{\bullet} \quad (1)$$

$$HO^{\bullet} + \text{organics} \rightarrow \text{intermediates} \rightarrow CO_2 + H_2O + ... \quad (2)$$

$$HO^{\bullet} + HO^{\bullet} \rightarrow H_2O_2 \quad (3)$$

$$h^+(TiO_2) + \text{organics} \rightarrow \text{intermediates} \rightarrow CO_2 + H_2O + \ldots \quad (4)$$

The behavior of phenol at the Ag-TiO_2/Ti nanotubes array photoanode was characterized by linear voltammetry. Fig. 5 shows linear voltammograms of Ag-TiO_2/Ti nanotubes array photoanode at luminescent light illumination. At 550 mV the phenol oxidation peaks were observed on the voltammetric curve. It could be noted that no oxidation peaks were observed on the voltammetric curves in the pure 0.1 M Na_2SO_4 solution. This demonstrates that Ag-TiO_2 nanotubes photoanode was stable under these conditions. Phenol was directly electrocatalytically oxidized on the surface of Ag-TiO_2/Ti nanotubes.

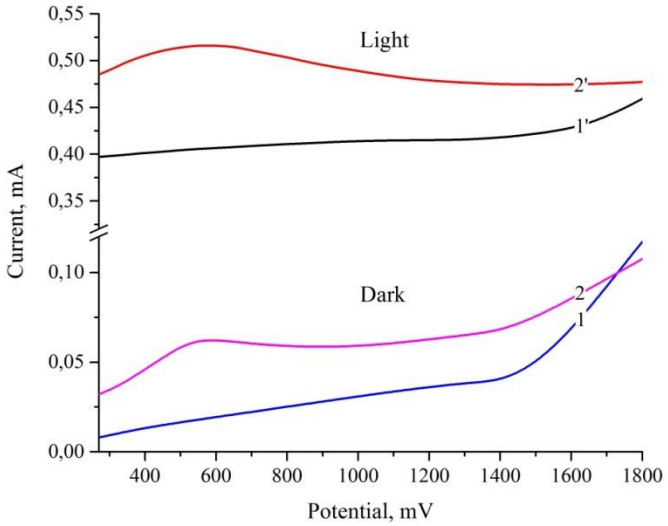

Figure 5. Linear voltammograms of Ag-TiO_2/Ti nanotubes array photoanode: 1, 1' – 0.1 M Na_2SO_4; 2, 2' - 0.1 M Na_2SO_4 with 10 $mg \cdot l^{-1}$ phenol (scan rate – 100 mV/s).

When phenol is added to a solution, by direct oxidation occurs the depletion layer of holes, which leads to increase the photocurrent. (Fig. 5). The reaction (1) is electrochemical, which produced the background photocurrent. The hydroxyl radicals react with each other lead to the production of H_2O_2 during the photoelectrocatalytic process, as strong oxidizing agent for the degradation of phenol (**3**). In addition, holes may directly oxidize phenol (4), adsorbed on the surface of TiO_2.

On Ag loaded TiO_2 nanotubes surface the photogenerated electrons flow toward Ag nanoparticles and react with oxygen to form $O_2^{\bullet-}$. The process can be used for decreasing recombination of photogenerated electrons and holes [40].

$$O_2 + e\text{-}(Me) \rightarrow O_2^{\bullet-} \quad (5)$$

In the presence of molecular oxygen as surface acceptors of electrons, the radical $O_2^{\bullet-}$ also formed hydroxyl radicals ($HO^{\bullet}$) according to the reaction [52,53]:

$$O_2^{\bullet-} + H^+ \rightarrow HO^{\bullet} \quad (6)$$

This mechanism suggested that the presence of oxygen was essential for photoelectrocatalytic oxidation of phenol. It allows an increase of hole lifetime by reaction with electron and the formation of oxidizing species OH· radicals.

The electrons are captured by the silver nanoparticles can react with Ho· radicals produced by reaction (**1**) and (**6**):

$$HO^{\bullet} + e^-(Me) \rightarrow HO^- \quad (7)$$

The reaction (**7**) leads to decrease the $HO^{\bullet}$ radicals in solution, therefore more phenol molecules will be oxidized through direct oxidation by holes. This will be to increase the photocurrent on the voltammetric curves of phenol oxidation on the Ag loaded TiO_2 nanotubes.

In accordance to this, we have investigated the effect of oxygen pressure on photoelectrocatalytic oxidation of phenol on Ag loaded TiO_2 nanotubes.

When the oxygen pressure is increased, photoelectrocatalytic phenol oxidation rate, corresponding to the peak height at 500 *mV*, has increased as shown in Fig. 6. This effect could be due

to the increased electrocatalytic activity of Ag-TiO_2/Ti nanotube array electrode, which in turn is responsible for the oxidation of the phenol molecules.

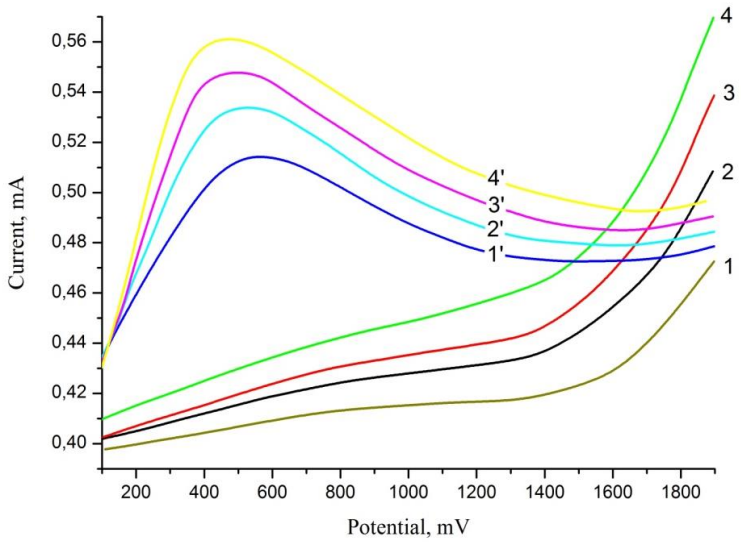

Figure 6. Linear voltammetric curves phenol photoelectrocatalytic oxidation on Ag-TiO_2/Ti nanotube array electrode with different oxygen pressure (MPa): 1' – 0.1; 2' – 0.2; 3' – 0.4; 4' – 0.6; 1-4 – 0.1 M Na_2SO_4 (C_{ph} = 10 mg·l^{-1}; Scan Speed – 100 mV/s).

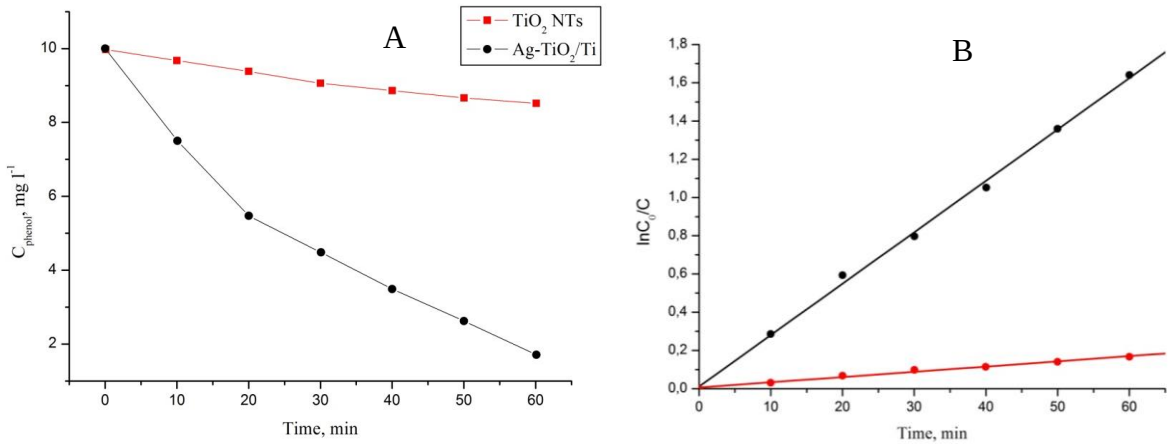

Figure 7. Photoelectrocatalytic oxidation of phenol using pure TiO_2 and Ag-loaded TiO_2 nanotubes (A) and its plot of ln C_0/C versus irradiation time (B).

The increase current on the voltammetric curves is caused by reaction (**5**). The rate of this reaction at high oxygen pressure increased which creates more holes. This leads to the preferential occurrence of the electrochemical reaction (**4**).

Figure 7 shows the photoelectrocatalytic oxidation of phenol on pure TiO_2 nanotubes and Ag-loaded TiO_2 nanotubes electrodes under luminescent light illumination. After 60 min luminescent light irradiation, the degradation rates of phenol on pure TiO_2 nanotubes and Ag loaded TiO_2 nanotubes were 15 and 83 %, respectively. The degree of phenol oxidation is about 15% for the pure TiO_2 nanotubes, apparently due to the oxidative adsorption of phenol on the surface photoanode [54,55].

Photoelectrocatalytic degradation efficiency of phenol over Ag loaded TiO_2 nanotubes was 83 %, higher than that of pure TiO_2 nanotubes sample.

In order to determine the order of the reaction, the photoelectrocatalytic oxidation reaction of phenol (C=10 $mg \cdot l^{-1}$) was carried out at pH=7.1. The rate constant for the photoelectrocatalytic oxidation of phenol was obtained from the first order rate equation (Eq. 1).

$$-\ln\frac{C_0}{C} = kt$$

where C and C_0 are the concentrations of the substrate at time *t* and time *0* in minutes, k is the first order rate constant (min^{-1}).

The plot of $\ln C_0/C$ versus treatment time shows a straight line behavior and the rate constants were determined from the slope of the straight line. The plot of $\ln C_0/C$ versus treatment time of photoelectrocatalytic oxidation of phenol on pure TiO_2 and Ag loaded TiO_2 nanotubes is shown in Fig. 7 (B). It shows that the photoelectrocatalytic oxidation proceeds through first order kinetics. The rate constants and the initial rate of phenol photoelectrocatalytic oxidation obtained for the pure TiO_2 and Ag loaded TiO_2 nanotubes are given in table 1. These results also show that the photoelectrocatalytic oxidation of phenol was faster on Ag loaded TiO_2 nanotubes than on pure TiO_2 nanotubes. Complete oxidation takes place within 120 *min* on the Ag loaded TiO_2 nanotubes photoanode. The initial rate of phenol photoelectrocatalytic oxidation is nearly ten times greater on the Ag loaded TiO_2 nanotubes photoanode than on pure TiO_2 nanotubes. A similar trend in the photoelectrocatalytic activity of pure and modified TiO_2 is observed in previous studies [56–58].

Table 1. Apparent rate constant k_{app} and initial rate for phenol photoelectrocatalytic oxidation

Photoanode	Rate constant, min^{-1}	Initial rate, R, $mg \cdot l^{-1} \cdot min^{-1}$
Ti/TiO_2	0.0027	0.027
$Ag\text{-}TiO_2/Ti$	0.0282	0.282

Inserting the effect of oxygen pressure to the photo electrocatalytic oxidation initial rate and degree of oxidation is important for developing the wastewater treatment at high pressure. The photoelectocatalytic oxidation of phenol at the different pressure ranging from 0.1 – 0.6 *MPa*, at a fixed concentration of phenol (10 $mg \cdot l^{-1}$) and time, has been investigated on Ag loaded TiO_2. Fig. 8 (A) shows the effect of oxygen pressure on the initial rate of phenol oxidation. Results show that the initial rate of oxidation increases with increasing oxygen pressure. The initial rate of photoelectrocatalytic phenol oxidation increased nearly 1.4 times by raising the oxygen pressure in the system from 0.1 to 0.6 *MPa*.

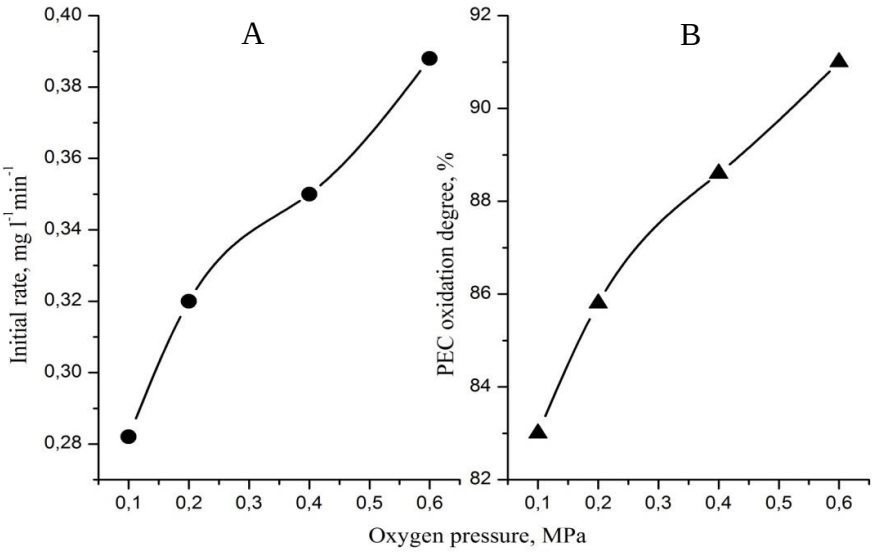

Figure 8. Effect of oxygen pressure on initial rate (A) and degree of photoelectrocatalytic oxidation of phenol (B).

Table 2. Comparison of the photoelectrocatalytic phenol degradation obtained in this study with the findings in the literature**.**

N	Photoanode	Conditions	Light Source	Phenol degradation degree, %	Reference
1	TiO_2/Ni thin-film electrode	Phenol – 100 $mg{\cdot}l^{-1}$ Time 3 *h*	300 W medium pressure mercury lamp	85	[59]
2	Multi-walled carbon nanotube-doped TiO_2	Phenol – 20 *ppm* 0.1 M $NaClO_4$	300 W UV-free Xe light system	58	[60]
3	Ti/TiO_2 doped with Ga^{3+}	Phenol –15,9 $mg{\cdot}l^{-1}$ Time 3 *h*	_	100	[61]
4	Ag loaded Ti/TiO_2	Phenol –10 $mg{\cdot}l^{-1}$ Time – 4 *h*	Luminescent lamp	96	This study

The mechanisms of photoelectrocatalytic phenol degradation on TiO_2 photoanodes have been discussed in papers [59–61]. Some research findings of various photoanode use for the degradation of phenol were compared and the result is tabulated in Table 2. It can be clearly observed that photoelectrocatalytic oxidation of phenol at high pressure is quite comparable to other results. The

photoelectrocatalytic oxidation of phenol on Ag-TiO2/Ti photoanode gave higher degradation percentages but required a high pressure and necessary appropriate equipment.

When photoelectrocatalytic oxidation of phenol at high oxygen pressure, in addition where molecular oxygen is used as an electron acceptor to trap and remove electrons from the surface of the titania, dissolved oxygen may be reduced directly on the cathode surface with the generation of hydrogen peroxide [62]. Increasing the molecular oxygen reduction reaction rate will increase the efficiency of photoelectrocatalytic oxidation of phenol. If the adsorbed oxygen is in excess on the cathode surface the rate of the electrochemical generation of hydrogen peroxide will be maximized [63]. Under these conditions the H_2O_2 is electrogenerated by a two-electron reduction of molecular oxygen [64].

This can be rationalized by considering the following: when the oxygen pressure is high, a rise of oxygen concentration in solution occurs and results in oxygen electroreduction, generating H_2O_2, HO_2^-, $O_2^{\bullet-}$ and other oxygen containing active species [65–67].

The oxygen reductions up to the hydrogen peroxide play an important role in an increased rate of photoelectrocatalytic oxidation of phenol, since hydrogen peroxide is electron acceptor and can decompose with the formation of a powerful oxidant, HO· radicals according to the reaction [68].

$$TiO_2\,(e^-) + H_2O_2 \rightarrow TiO_2 + OH^- + HO^{\bullet} \quad (8)$$

Since hydrogen peroxide is a better electron acceptor than molecular oxygen, it could act as an alternate for oxygen and hence enhanced degradation will be observed.

Fig. 8 (B) shows that percentage of phenol oxidation increases as the oxygen pressure increases under luminescent light illumination. This figure depicts the influence of oxygen pressure on phenol removal during the photoelectrocatalytic process using Ag loadedTiO_2 nanotube anode and platinum cathode in 0.1 M Na_2SO_4 electrolyte. The oxidation degree is directly proportional to the oxygen pressure and the phenol removal efficiency increases when the oxygen pressure of 0,6 MPa was used. This corresponds not only an increase the rate of the trap and removes electrons from the surface of the titania, but also increase the electrogenerated of H_2O_2 [69].

4. CONCLUSION

The results of our study show the role of the silver dopant in enhancing photoelectrocatalytic activity of TiO_2 nanotubes under visible light irradiations. Surface modification of nanoparticles of TiO_2 nanotubes by Ag also promotes efficient charge separation in the system. In this case, it is shown that by combining of the modification of TiO_2 nanotubes surface by Ag nanoparticles, the pressurized oxygen can provide efficient photoelectrocatalytic oxidation of phenol. The increased oxygen pressure intensifies the photoelectrocatalytic oxidation of phenol, since oxygen is the electron acceptor, it captures one or two of photogenerated electrons from the surface of the photocatalyst, as a result, holes can freely diffuse to the semiconductor surface and oxidize the adsorbed phenol. Increase the efficiency photoelectrocatalytic oxidation of phenol under oxygen pressure caused by the participation of dissolved oxygen in photocatalytic and electrochemical processes. The participation of oxygen on the surface of Ag loaded TiO_2 nanotubes in the photocatalytic process decreases the rate of electron-

hole recombination. In addition, the dissolved oxygen is reduced to the hydrogen peroxide at the cathode surface, which also improves the efficiency of the process.

ACKNOWLEDGEMENT
This study was funded by the Ministry of Education and Science of the Russian Federation as part of state assignment number 2560, project (Grant Number: 16.1103.2014/K) and Dagestan State University Strategic Development Program.

References

1. S. Ichikawa, R. Doi, *Catal. Today*, 27 (1996) 271.
2. I.U. Haque, J.F. Rusling, *Chemosphere*, 26 (1993) 1301.
3. D. H. Kim, M. A. Anderson, *Environ. Sci. Technol*., 28 (1994) 479.
4. K. Vinodgopal, S. Hotchandani, P.V. Kamat, *J. Phys. Chem*., 97 (1993) 9040.
5. K. Nakata, A. Fujishima, *J. Photochem. Photobiol. C Photochem. Rev*., 13 (2012) 169.
6. X. Chen, S. S. Mao, *Chem. Rev.*, 107 (2007) 2891.
7. M. Pelaez, N.T. Nolan, S.C. Pillai, M.K. Seery, P. Falaras, A.G. Kontos, P.S.M.Dunlop, J.W.J. Hamilton, J.A. Byrne, K. O'Shea, M.H. Entezari and D.D.Dionysiou, *Appl. Catal. B Environ.*, 125 (2012) 331.
8. M. R. Bayati, F. Golestani-Fard, A.Z. Moshfegh, *Mater. Chem. Phys*., 120 (2010) 582.
9. I.K. Konstantinou, T.A. Albanis, *Appl. Catal. B Environ*., 49 (2004) 1.
10. V. Galstyan, E. Comini, G. Faglia and G. Sberveglieri, *Sensors*, 13 (2013) 14813.
11. M. Paulose, H.E. Prakasam, O.K. Varghese, L. Peng, K.C. Popat, G.K. Mor, T.A. Desai and C.A. Grimes, *J. Phys. Chem. C.*, 111 (2007) 14992.
12. U. Diebold, *Surf. Sci. Rep.*, 48 (2003) 53.
13. S.P. Albu, A. Ghicov, J.M. Macak and P. Schmuki, *Phys. Status Solidi – Rapid Res. Lett.*, 1 (2007) R65.
14. D. Gong, C. Grimes, O. K. Varghese, W. Hu, R. S. Singh, Z. Chen and E.C. Dickey, *J. Mater. Res*., 16 (2001) 3331.
15. G.K. Mor, O.K. Varghese, M. Paulose, N. Mukherjee and C.A. Grimes, *J. Mater. Res*., 18 (2011) 2588.
16. G.K. Mor, K. Shankar, M. Paulose, O.K. Varghese and C.A. Grimes, *Nano Lett*., 6 (2006) 215.
17. G.K. Mor, O.K. Varghese, M. Paulose, K. Shankar and C.Grimes, *Sol. Energy Mater*. Sol. Cells, 90 (2006) 2011.
18. J. Fang, F. Wang, K. Qian, H. Bao, Z. Jiang and W. Huang, *J. Phys. Chem. C.*, 112 (2008) 18150.
19. C. Zhang, U. Chaudhary, D. Lahiri, A. Godavarty and A. Agarwal, *Scr. Mater*., 68 (2013) 719.
20. W. Shu, Y. Liu, Z. Peng, K. Chen, C. Zhang and W. Chen, *J. Alloys Comp*., 563 (2013) 229.
21. E. Bae, W. Choi, *Environ. Sci. Technol*., 37 (2003)147.
22. P. Kittisakmontree, B. Pongthawornsakun, H. Yoshida, S. Fujita and M. Arai, *J. Panpranot, J. Catal.*, 297 (2013) 155.
23. G.L. Chiarello, M.H. Aguirre, E. Selli, *J. Catal*., 273 (2010) 182.
24. G. Colón, M. Maicu, M.C. Hidalgo and J. Navío, *Appl. Catal. B Environ*., 67 (2006) 41.
25. A. Roguska, A. Kudelski, M. Pisarek, M. Opara and M. Janik-Czachor, *Appl. Surf. Sci.*, 257 (2011) 8182.
26. L. Gao, W. Gan, S. Xiao, X. Zhan and J. Li, *Ceram. Int*., 42 (2016) 2170.
27. J. Ma, X. Guo, Y. Zhang, H. Ge, *Chem. Eng. J.*, 258 (2014) 247.
28. L. Mai, D. Wang, S. Zhang, Y. Xie, C. Huang and Z. Zhang, *Appl. Surf. Sci*., 257 (2010) 974.
29. M. J. Nalbandian, M. Zhang, J. Sanchez, S. Kim, Y. H. Choa, D. M. Cwiertny and N.V. Myung, *J.*

Hazard. Mater., 299 (2015) 141.
30. S.Y. Ryu, J.W. Chung, S.Y. Kwak, *Compos. Sci. Technol*., 117 (2015) 9.
31. X. Li, F. Wang, Q. Qian, X. Liu, L. Xiao and Q. Chen, *Mater. Lett*., 66 (2012) 370.
32. G. Guo, B. Yu, P. Yu, X. Chen, *Talanta*, 79 (2009) 570.
33. T. Sun, E. Liu, J. Fan, X. Hu, F. Wu, W. Hou, Y. Yang and L. Kang, *Chem. Eng. J*., 228 (2013) 896.
34. J. Ma, M. Yang, Y. Sun, C. Li, Q. Li, F. Gao, F. Yu and J. Chen, *Phys. E Low-Dimensional Syst. Nanostructures*, 58 (2014) 24.
35. K. Chen, X. Feng, R. Hu, Y. Li, K. Xie, Y. Li and H. Gu, *J. Alloys Comp*., 554 (2013) 72.
36. Y. Lai, H. Zhuang, K. Xie, D. Gong, Y. Tang, L. Sun, C. Lin and Z. Chen, *New J. Chem*., 34 (2010) 1335.
37. X. Liu, Z. Liu, J. Lu, X. Wu, B. Xu and W. Chu, *Appl. Surf. Sci*., 288 (2014) 513.
38. F.F. Orudzhev, Z.M. Aliev, F.G. Gasanova, A.B. Isaev and N.S. Shabanov, *Russ. J. Electrochem.*, 51 (2015) 1247.
39. F.F. Orudzhev, F.G. Gasanova, Z.M. Aliev and A.B. Isaev, *Nanotechnologies in Russia*, 7 (2012) 482.
40. G. Xu, H. Liu, J. Wang, J. Lv, Z. Zheng and Y. Wu, *Electrochim. Acta*, 121 (2014) 194.
41. C. Turchi, D. F. Ollis, *J. Catal.*, 122 (1990) 178.
42. E. Kowalska, H, Remita, C. Colbeau-Justin, J. Hupka, J. Belloni, *J. Phys. Chem. C*., 112 (2008) 1124.
43. O.T. Alaoui, A. Herissan, C. Le Quoc, M. el Mehdi Zekri, S. Sorgues, H. Remita and C. Colbeau-Justin, *J. Photochem. Photobiol. A Chem*., 242 (2012) 34.
44. J. Fang, F. Wang, K. Qian, H. Bao, Z. Jiang and W. Huang, *J. Phys. Chem. C.*, 112 (2008) 18150.
45. T. Wu, S. Liu, Y. Luo, W. Lu, L. Wang, X. Sun, *Nanoscale*, 3 (2011) 2142.
46. Z. Lian, W. Wang, S. Xiao, X. Li, Y. Cui, D. Zhang, G. Li and H. Li, *Sci Rep*., 5 (2015) 10461.
47. A.L. Luna, D. Dragoe, K. Wang, P. Beaunier, E. Kowalska, B. Ohtani, D.B. Uribe, M.A. Valenzuela, H. Remita and C. Colbeau-Justin, *J. Phys. Chem. C.*, 121 (2017) 14302–.
48. S. Malato, P. Fernández-Ibáñez, M.I. Maldonado, J. Blanco and W. Gernjak, *Catal. Today*, 147 (2009) 1.
49. J.M. Herrmann, *Catal. Today*, 53 (1999) 115.
50. H. Wang, J. Li, X. Quan, Y. Wu, *Appl. Catal. B Environ*., 83 (2008) 72.
51. M. Kubo, K. Matsuoka, A. Takahashi, N. Shibasaki-Kitakawa and T. Yonemoto, *Ultrason. Sonochem.*, 12 (2005) 263.
52. K. Chhor, J.F. Bocquet, C. Colbeau-Justin, *Mater. Chem. Phys.*, 86 (2004) 123.
53. A.L. Linsebigler, G. Lu, J.T. Yates Jr, *Chem. Rev.*, 95 (1995) 735.
54. Z. Wang, W. Cai, X. Hong, X. Zhao, F. Xu and C. Cai, *Appl. Catal. B Environ*., 57 (2005) 223.
55. S. Bekkouche, M. Bouhelassa, N.H. Salah and F.Z. Meghlaoui, *Desalination*, 166 (2004) 355.
56. J. Li, N. Lu, X. Quan, S. Chen, H. Zhao, *Ind. Eng. Chem. Res*., 47 (2008) 3804.
57. D.F. Ollis, C.Y. Hsiao, L. Budiman and C.L. Lee, *J. Catal*., 88 (1984) 89.
58. X.Z. Li, H.L. Liu, P.T. Yue and Y.P. Sun, *Environ. Sci. Technol*., 34 (2000) 4401.
59. Y. Xiaoli, S. Huixiang, W. Dahui, *Korean J. Chem. Eng*., 20 (2003) 679.
60. L.C. Chen, Y.C. Ho, W.S. Guo, C.M. Huang and T.C. Pan, *Electrochim. Acta*, 54 (2009) 3884.
61. L.S. Andrade, E.A. Laurindo, R.V.D. Oliveira, R.C. Rocha-Filho and Q.B. Cass, *J. Braz. Chem. Soc.*, 17 (2006) 369.
62. A. Alverez-Gallegos, D. Pletcher, *Electrochim. Acta*, 44 (1999) 2483.
63. Z. Shen, J. Yang, X. Hu, Y. Lei, X. Ji, J. Jia and W. Wang, *Environ. Sci. Technol*., 39 (2005) 1819.
64. Z. Qiang, J.H. Chang, C.P. Huang, *Water Res*., 36 (2002) 85.
65. I. Ilisz, Z. László, A. Dombi, *Appl. Catal. A Gen*., 180 (1999) 25.
66. E. Yeager, *Electrochim. Acta*, 29 (1984) 1527.
67. M. S. Hossain, D. Tryk, E. Yeager, *Electrochim. Acta*, 34 (1989) 1733.

68. A.V. Rupa, D. Manikandan, D. Divakar and T. Sivakumar, *J. Hazard. Mater*., 147 (2007) 906.
69. R.J. Ramírez, C.A. Arellano, A.A. Gallegos, A.E. González and S.S. Martínez, J. *Photochem. Photobiol. A Chem*., 305 (2015) 51.